

Available online at [www.sciencedirect.com](http://www.sciencedirect.com)

Nuclear Physics B 824 (2010) 254–272

[www.elsevier.com/locate/nuclphysb](http://www.elsevier.com/locate/nuclphysb)

# Simulating the all-order strong coupling expansion III: $O(N)$ sigma/loop models

Ulli Wolff<sup>1</sup>*Institut für Physik, Humboldt Universität, Newtonstr. 15, 12489 Berlin, Germany*

Received 10 August 2009; accepted 2 September 2009

Available online 6 September 2009

---

## Abstract

We reformulate the  $O(N)$  sigma model as a loop model whose configurations are the all-order strong coupling graphs of the original model. The loop configurations are represented by a pointer list in the computer and a Monte Carlo update scheme is proposed. Sample simulations are reported and the method turns out to be similarly efficient as the reflection cluster method, but it has greater potential for systematic generalization to other lattice field theories. A variant action suggested by the method is also simulated and leads to a rather extreme demonstration of the concept of universality of the scaling or continuum limit.

© 2009 Elsevier B.V. All rights reserved.

---

## 1. Introduction

The family of globally  $O(N)$  invariant nonlinear sigma models, also called  $N$ -vector models, are very important statistical systems. For obvious reasons, in three space dimensions, they play a very prominent rôle in condensed matter physics. We here only mention the XY model ( $N = 2$ ), relevant for the description of liquid helium, and the Heisenberg model ( $N = 3$ ) for magnets. In high energy physics the four dimensional versions appear as effective field theories, for instance for pion physics, and a lot of interest focuses also on two (Euclidean) dimensions. This is motivated by the fact that these field theories are asymptotically free and share features with QCD like asymptotic freedom and dimensional transmutation with the nonperturbative generation of

---

*E-mail address:* [uwolff@physik.hu-berlin.de](mailto:uwolff@physik.hu-berlin.de).

<sup>1</sup> I would like to dedicate this paper to Martin Lüscher on the occasion of his sixtieth birthday. I thank him for his superb contributions to quantum field theory and for the privilege to collaborate with him.

a scale like  $\Lambda_{\text{QCD}}$ . For example the study of a nonperturbative renormalized coupling constant in [1] was an important preparation for the QCD Schrödinger functional methods [2].

With regard to the technique of Monte Carlo simulation, our main access to the models beyond perturbation theory, since about 20 years we are in an exceptional situation with regard to the  $O(N)$  models. The method of cluster updates [3] for embedded  $Z(2)$  (Ising) degrees of freedom [4] allows to painlessly enter the critical region, which unfortunately is in stark contrast to our possibilities in QCD. The hope that the cluster method would be widely generalizable was unfortunately disappointed in the following years, at least for high energy physics. In [5] even a kind of ‘heuristic<sup>2</sup> no-go theorem’ was given concerning the generalization to sigma models with other spin manifolds. With the advent (or rather recognition<sup>3</sup>) of [6] a completely different strategy to overcome slowing down has appeared: Simulate the strong coupling graphs (to arbitrary order) instead of field configurations. Close to criticality the relevant field configurations are long-distance correlated. The cluster method, using an auxiliary percolation process, manages to execute collective moves that are thermodynamically appropriate for this case. Such moves seem to be difficult to find (and implement efficiently) in general.<sup>4</sup> The strong coupling graphs that are relevant at criticality are large and numerous. The clever idea of Prokof’ev and Svistunov [6] was to generate them not for the partition function alone, but to simultaneously consider the two point correlation. They have demonstrated in simple models that local deformations can pass between such graphs without significant obstructions and thus a relevant sample can be simulated. To avoid confusion we remind the reader of the following. In ordinary strong coupling expansions one takes the thermodynamic limit term by term and then the series usually has a finite radius of convergence which is often related to phase transitions. A finite lattice regularizes such singularities (for compact fields at least) and we can compute everything to in principle arbitrary precision by a convergent expansion for arbitrary couplings or temperature. While close to criticality this is impractical by conventional systematic expansion the stochastic evaluation is feasible. We may now also speak about an equivalence with another statistical system which incidentally has only discrete variables. Note that, although there are some similarities, this is not a complete duality transformation in the sense of Kramers and Wannier [8].

In a recently begun series of papers [9,10] we have started to further work out the new approach. Beyond the Ising model we could apply it to fermions. Due to the sign problem this is at the moment still restricted to two dimensional systems like the Gross–Neveu model [11]. A novelty that one has to appreciate is that the generated graphs can be adapted to the observables that one is interested in. One then needs several simulations for different quantities. We nonetheless see these dedicated simulations as a strength of the method. In [9,12,11] it was found that this extra effort can result in enhanced precision for interesting observables.

In this article we successfully extend the all-order strong coupling method to the class of  $O(N)$  nonlinear sigma models in arbitrary dimension. We first achieve this for the standard lattice action which allows to confirm our results by comparing to other data in the literature. While the standard action has a relatively complicated all-order expansion we can define another action by insisting on a simpler expansion. Formally it can be argued to lie in the same universality class, but on the other hand it looks like a rather radical mutilation of the original spin model. We simulate its graphs and find that at least one universal result is reproduced quite accurately

---

<sup>2</sup> There are mathematical proofs which refer however to smooth field configurations.

<sup>3</sup> I am indebted to Urs Wenger in this context.

<sup>4</sup> See [7] for a recent new proposal in this direction.

and universality is confirmed. This flexibility will hopefully be useful to tackle further more complicated models in the future.

In Section 2 we develop the loop model equivalent to the all-order expansion of the  $O(N)$  system. In Section 3 we discuss how to represent the loop configurations in the computer and how to sample them. Extensive tests with the standard action are carried out in Section 4. Section 5 discusses universality and the modified action followed by conclusions in Section 6. In Appendix A the limit  $N = 1$  of our algorithm and its relation to previous Ising work is discussed.

## 2. $O(N)$ model as a loop ensemble

We consider spin models with  $N$  component spins  $s(x)$  of unit length located at the sites of a  $D$  dimensional hypertorus of length  $L_\mu$  in the various directions. We refer all lengths to the isotropic lattice spacing thus putting  $a = 1$ . For the standard lattice action the partition function with two field insertions reads

$$Z(u, v) = \int \left[ \prod_z d\mu(s(z)) \right] e^{\beta \sum_{l=\langle xy \rangle} s(x) \cdot s(y)} s(u) \cdot s(v). \tag{1}$$

The sum is over nearest neighbor links and the dots between pairs of spins mean  $O(N)$  invariant scalar products. The integrations employ the normalized  $O(N)$  invariant measure on the sphere,

$$\int d\mu(s) f(s) = K_N \int d^N s \delta(s^2 - 1) f(s), \quad K_N \leftrightarrow \int d\mu(s) = 1. \tag{2}$$

Later on we shall need the corresponding single site generating function for a general source  $j_\alpha$

$$\int d\mu(s) e^{j \cdot s} = G_N(j) = \sum_{n=0}^{\infty} c[n; N] (j \cdot j)^n \tag{3}$$

which is essentially given by the modified Bessel function  $I_{N/2-1}$  and has expansion coefficients

$$c[n; N] = \frac{\Gamma(N/2)}{2^{2n} n! \Gamma(N/2 + n)}. \tag{4}$$

The strong coupling expansion in  $\beta$  is generated by independently summing over an integer link field  $k(l) = 0, 1, 2, \dots, \infty$  in

$$Z(u, v) = \sum_k \int \left[ \prod_z d\mu(s(z)) \right] \prod_{l=\langle xy \rangle} \frac{\beta^{k(l)}}{k(l)!} [s(x) \cdot s(y)]^{k(l)} s(u) \cdot s(v). \tag{5}$$

For a given configuration  $k$  the spin integral may now be written as

$$X = \frac{\partial}{\partial j_\alpha(u)} \frac{\partial}{\partial j_\alpha(v)} \prod_{l=\langle xy \rangle} \left[ \frac{\partial}{\partial j_\gamma(x)} \frac{\partial}{\partial j_\gamma(y)} \right]^{k(l)} \prod_z G_N(j(z)) \Big|_{j=0}. \tag{6}$$

We next introduce an auxiliary integer site field

$$d(x) = \delta_{x,u} + \delta_{x,v} + \sum_{l, \partial l \ni x} k(l) \tag{7}$$

which counts the number of spins or respectively  $j$ -derivatives at  $x$ . It as well as  $X$  depends on  $u, v, k$ , of course, which we leave implicit for easier notation. To produce a nonzero  $X$ ,  $d(x)$

has to be even on all sites. Then the contribution becomes

$$X' = \frac{\partial}{\partial j_\alpha(u)} \frac{\partial}{\partial j_\alpha(v)} \prod_{l=\langle xy \rangle} \left[ \frac{\partial}{\partial j_\gamma(x)} \frac{\partial}{\partial j_\gamma(y)} \right]^{k(l)} \prod_z [j(z) \cdot j(z)]^{d(z)/2} \tag{8}$$

where there are as many  $j$  factors as there are derivatives. In addition  $X'$  differs from  $X$  by dropping factors  $c[d(z)/2; N]$  for all sites  $z$ . The total number of terms in  $X'$  from taking all derivatives is

$$\mathcal{M}_0[u, v; k] = \prod_z d(z)! \tag{9}$$

The terms differ in their  $O(N)$  index contraction structures. Each of them can be represented by a graph  $\Lambda$  drawn on the lattice. There are  $k(l)$  lines between each nearest neighbor pair  $\langle xy \rangle = l$ . At the ‘interior of the sites’ there is a kind of switch-board that sets up pairwise connections between all surrounding lines. Only at  $u$  and  $v$  two lines are left unpaired locally and instead are contracted with each other. Thus all lines are arranged in closed loops. The chain between  $u$  and  $v$  does not close geometrically (unless  $u = v$ ) but closes with respect to  $O(N)$  contractions leading to factor  $N$  as all other loops do. In the next section a visualization of such a graph or loop configuration will be given. Each graph with a definite ‘switchboard’ configuration still appears many times among the  $\mathcal{M}_0$  terms. This multiplicity is

$$\mathcal{M}[u, v; k] = \left( \prod_l k(l)! \right) \prod_x [d(x)/2]! 2^{d(x)/2} \tag{10}$$

due to the possibility of permuting within a graph the connecting lines on the links, the pairs  $j \cdot j$  at the sites and the two factors in each pair. The total number of different graphs (for given  $u, v, k$ ) is hence equal to  $\mathcal{M}_0/\mathcal{M}$ . So far we have considered the loop configurations for given  $u, v, k$ . It is clear however, that the latter are also determined by the graph on the lattice. We may hence independently sum over graphs  $\Lambda \in \mathcal{L}_2$  which we define to include all possible locations  $u, v$  of the two ‘defects’ and all possible  $k(l)$  assignments to links that produce nonvanishing contributions. Then from (5) we generalize to

$$\mathcal{Z} = \sum_{u,v} \rho^{-1}(u-v) Z(u, v) = \sum_{\Lambda \in \mathcal{L}_2} \rho^{-1}(u-v) W[\Lambda] \tag{11}$$

where we have collected the whole loop weight into

$$\begin{aligned} W[\Lambda] &= N^{|\Lambda|} \mathcal{M}[u, v; k] \left[ \prod_{l=\langle xy \rangle} \frac{\beta^{k(l)}}{k(l)!} \right] \prod_z c[d(z)/2; N] \\ &= N^{|\Lambda|} \beta^{\sum_l k(l)} \left[ \prod_x 2^{-d(x)/2} \frac{\Gamma(N/2)}{\Gamma(N/2 + d(x)/2)} \right]. \end{aligned} \tag{12}$$

Here  $u, v, k(l)$  and thus  $d(x)$  are now functions of  $\Lambda$ , and  $\rho$  is a positive weight to be chosen later. In the exponent  $|\Lambda|$  means the number of individual closed loops including the  $u-v$  chain. The loops in the configurations  $\Lambda$  that we sum over can overlap, intersect and backtrack. The weight depends on these features, the loops interact. In the next section we shall introduce an explicit parameterization of  $\Lambda$  together with an update scheme to simulate the loop model.

As a by now standard next step [9] we introduce expectation values with respect to the new ensemble

$$\langle\langle A(\Lambda) \rangle\rangle = \frac{1}{\mathcal{Z}} \sum_{\Lambda \in \mathcal{L}_2} \rho^{-1}(u-v) W[\Lambda] A(\Lambda). \quad (13)$$

For the two point function of the original model there is the trivial relation

$$\langle s_\alpha(u) s_\beta(v) \rangle = \frac{\delta_{\alpha\beta}}{N} \frac{Z(u, v)}{Z(\emptyset)} \quad (14)$$

where  $Z(\emptyset)$  is the partition function without insertions (or  $u = v$ ). This ratio can obviously be obtained from (13) as

$$\langle s_\alpha(0) s_\beta(x) \rangle = \frac{\delta_{\alpha\beta}}{N} \rho(x) \frac{\langle\langle \delta_{u-v, x} \rangle\rangle}{\langle\langle \delta_{u, v} \rangle\rangle} \quad (15)$$

where we have assumed the normalization

$$\rho(0) = 1. \quad (16)$$

It is convenient to in addition introduce expectation values referring to the subset of ‘vacuum’ configurations  $\Lambda \in \mathcal{L}_2$  that have  $u = v$ ,

$$\langle\langle A(\Lambda) \rangle\rangle_0 = \frac{\langle\langle \delta_{u, v} A \rangle\rangle}{\langle\langle \delta_{u, v} \rangle\rangle}. \quad (17)$$

Such expectation values are independent of the choice of  $\rho$ .

The internal energy density is equivalent to the average of the nearest neighbor correlation

$$E = \frac{1}{N_l} \sum_{l=(xy)} \langle s(x) \cdot s(y) \rangle \leq 1 \quad (18)$$

where  $N_l$  is the total number of links. By differentiating  $Z(\emptyset) = \mathcal{Z} \langle\langle \delta_{u, v} \rangle\rangle$  in both representations with respect to  $\beta$ , the relation

$$\beta E = \frac{1}{N_l} \sum_l \langle\langle k(l) \rangle\rangle_0 := K \quad (19)$$

follows easily. Thus the average link occupation is bounded by  $\beta$ . Numerical experience and large  $N$  considerations have shown that deep in the critical regime  $\beta/N$  are typically numbers smaller than one. Thus, although the total length of the loops in  $\Lambda$  is unbounded in principle, as an extensive quantity it will in practice never exceed the number of links on the lattice (times  $N$ ) by a large factor. We will come back to this point when we simulate. Another standard observable is the susceptibility

$$\chi = \sum_x \langle s(0) \cdot s(x) \rangle = \frac{\langle\langle \rho(u-v) \rangle\rangle}{\langle\langle \delta_{u, v} \rangle\rangle} \quad (20)$$

which follows from contracting and summing over  $x$  in (15).

The representation derived here allows to actually set  $N$  also to non-integer values. The value  $N = 1$  corresponds to the Ising model. The limit  $N \rightarrow 1$  of the present method does not immediately coincide with [6,9]. Therefore in Appendix A we discuss the connection.

### 3. Parameterizing and simulating the loop ensemble

#### 3.1. Parameterization: Loops as lists

It is often fruitful to first analyze graphs in an abstract manner and to separately consider their embedding on the lattice [13]. At the abstract level each graph  $\Lambda \in \mathcal{L}_2$  consists of lines and 2-vertices where two lines meet complemented with exactly two additional 1-vertices from the field insertions. We label all vertices with distinct integers. The lines are then naturally associated with pairs of integers. A valid embedding on the lattice associates lattice sites with vertices such that all lines map onto links, i.e. their index pairs refer to nearest neighbor sites. The 1-vertices are at the sites  $u$  and  $v$  which can be anywhere on the lattice.

We have found a representation for any embedded graph that we outline now. This is by no means unique. Our representation will actually be quite redundant by including extra information that will be found useful when we set up an update scheme in the next subsection. With any  $\Lambda$  we associate a list  $\ell$  which can be viewed as matrix  $\ell_{ij}$ . It has one row for each vertex of the graph and there are five columns. In our convention the first and second row are permanently associated with the 1-vertices at  $u$  and  $v$ . The remaining rows then deal with 2-vertices and the row-indices  $i$  are taken as the graph theoretic labels of the vertices. In the first column  $\ell_{i1}$  we encode the lattice site where the vertex is embedded. To this end we label the sites with integers  $1, 2, \dots, V$  in some order, with the lattice volume given by

$$V = \prod_{\mu} L_{\mu}. \tag{21}$$

Rows  $i$  of the list that are not in use for the given graph have  $\ell_{i1} = 0$ . The configuration  $\Lambda$  in general holds many closed loops. The columns  $\ell_{i2}$  and  $\ell_{i3}$  are filled such they allow to travel around the loop containing a vertex  $i$  by following the pointers

$$i \rightarrow i' = \ell_{i2} \rightarrow i'' = \ell_{i'2} \rightarrow \dots \rightarrow i. \tag{22}$$

The loop passing through  $i$  can be traveled in two possible directions of which one is given by column 2. By using column 3 one obtains the other direction. Note that the loops of the  $O(N)$  models are physically unoriented, and we here encounter one of the redundancies mentioned before. The chain between  $u$  and  $v$  is treated analogously with the exception that the journeys are  $1 \rightarrow i' = \ell_{12} \rightarrow i'' = \ell_{i'2} \rightarrow \dots \rightarrow 2$  and  $2 \rightarrow i' = \ell_{23} \rightarrow i'' = \ell_{i'3} \rightarrow \dots \rightarrow 1$ . From here on we call this special sequence of vertices and lines the active loop<sup>5</sup> with the remaining ones being called passive. Column 4 just holds a flag whose values distinguish vertices in passive loops (one) from those in the active loop (zero). Finally column 5 is arranged such that the following problem can be solved efficiently, i.e. without searching the whole list: for a given lattice site<sup>6</sup>  $x$  find all vertices (row-indices) embedded at this site for the present  $\Lambda$ . With an additional entry-list  $e(x)$  the problem is solved by following the sequence

$$x \rightarrow e(x) = i \rightarrow i' = \ell_{i5} \rightarrow i'' = \ell_{i'5} \rightarrow \dots. \tag{23}$$

This chain ends when  $\ell_{j5} = 0$  is encountered. During the later update a vertex can be removed from a graph. If it corresponds to row  $i$ , we set  $\ell_{i1} = 0$  in such a case. Such a row can continue

<sup>5</sup> Remember it is a closed loop in the  $O(N)$  sense yielding a factor  $N$ .

<sup>6</sup> By  $x$  we designate both the geometric location as well as the counting label given to it.

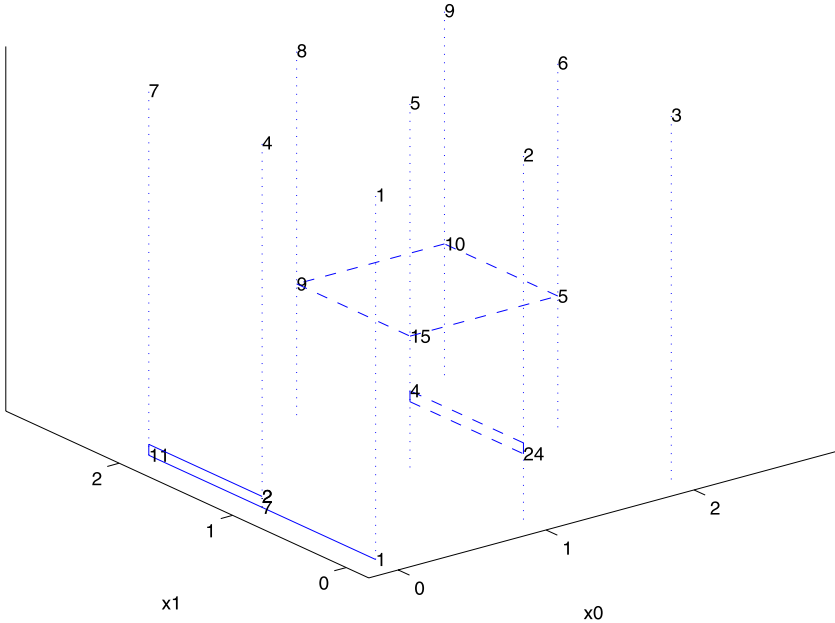


Fig. 1. A small loop configuration to illustrate its representation by a list.

however to function in (23). As a consequence, in (23) we can step through such lines which are still needed even without holding a vertex. In addition to  $\ell$  and  $e$  we also store the auxiliary field  $d(x)$ , although it could be constructed from  $\ell$ .

We now discuss as an example a  $3 \times 3$  lattice taken from an  $O(3)$  run. It is tiny to save space but it actually demonstrates most features. A loop configuration is shown in Fig. 1. We have displaced the loops in the third direction to disentangle overlapping loops. On the ‘roof’ we show the labeling of lattice sites, the other integers are vertex labels. The solid line, connecting 1 with 2 (via 7 and 11) is the active loop and there are two additional closed passive loops which overlap at site 5.

As already mentioned there is no hard bound on the number of rows/vertices that are needed in  $\ell$ . In addition, as  $A$  is updated (modified), vertices are added and eliminated and thus rows of  $\ell$  are freed (possibly with the exception of the entry in column 5) and new ones are required. As the available storage is finite, this requires some management which may seem difficult at first sight. Luckily this problem can be handled rather easily.

As argued before the average total number of vertices will be of order  $N \times N_l$ . As an extensive quantity its fluctuations are found to be only of the order  $\sqrt{N \times N_l}$ . We thus found that reserving space for

$$\{\ell_{i,j=1,\dots,5}\}, \quad i = 1, 2, \dots, f_\ell \times NN_l \tag{24}$$

lines with  $f_\ell$  of order unity leads to completely negligible probabilities to ever exhaust this space in any feasible simulation. These storage requirements are quite similar to ordinary simulations. By observing the fluctuations of  $\sum_x d(x)$  one can easily demonstrate failure probabilities like for example  $10^{-1000}$  which can be tolerated. We come back to this in Section 4.

For recycling list entries we keep another list with a reservoir of indices of completely unused rows that are available for new vertices. There is a subtlety here. As mentioned before a line not

Table 1

The list  $\ell$  corresponding to the configuration in Fig. 1 (upper two parts). It has been augmented by the leftmost (zeroth) column exhibiting the row indices. Completely unused lines have been omitted. The lower list is the entry table  $e(x)$ .

1	1	7	0	0	0									
2	4	0	11	0	0				10	9	9	5	1	22
3	0	21	1	0	24				11	7	2	7	0	17
4	5	24	24	1	15				12	0	2	1	0	0
5	6	10	15	1	8				15	5	5	9	1	6
6	0	9	1	0	0				16	0	17	17	0	0
7	4	11	1	0	16				17	0	7	7	0	0
8	0	22	1	0	0				22	0	9	5	0	0
9	8	15	10	1	0				24	2	4	4	1	0
						1	2	3	4	5	6	7	8	9
						12	3	0	7	4	5	11	9	10

carrying a vertex anymore can still be relevant as a ‘stepping stone’ in (23). Such rows we call ‘unused’ as opposed to ‘completely unused’. If we run out of completely unused rows during a simulation we start a recycling routine which runs through the whole list. In this process all  $\ell_{i5}$  where  $\ell_{i1} \neq 0$  and the associated entries in  $e$  are recomputed and all rows with  $\ell_{i1} = 0$  acquire the ‘completely unused’ status. It turns out that the time spent for list recycling is a negligible fraction of the total in practice. We end this subsection by reproducing in Table 1 the lists  $\ell$  and  $e$  associated with the configuration in Fig. 1.

### 3.2. Monte Carlo algorithm

We now propose an algorithm to simulate the  $O(N)$  loop ensemble (13). We define a number of separate update steps such that each of them fulfills detailed balance. They will then be iterated in some order as the final update procedure. The moves are all Metropolis proposals for which we quote the ratio  $q$  of the total weight in (13) after and before the move. They are accepted with the probability  $\min(1, q)$  in each case. We need to introduce the notion that the active loop between  $u$  and  $v$  is called trivial if it contains no 2-vertex and also  $u = v$  coincide.

- I. Extension and retraction: We choose with equal probability between  $2D + 1$  possible proposals to move  $u$  by one lattice spacing with a concurrent adjustment of the active loop. In the first  $2D$  cases it is extended with  $u$  moving to its neighbors  $\tilde{u}$  with the amplitude ratio

$$q_{\text{ext}} = \frac{\beta}{N + d[\tilde{u}]} \frac{\rho(u - v)}{\rho(\tilde{u} - v)}. \tag{25}$$

In the last case  $u$  is retracted by one link along the active loop with the ratio

$$q_{\text{ret}} = \frac{N + d[u] - 2}{\beta} \frac{\rho(u - v)}{\rho(\tilde{u} - v)}. \tag{26}$$

No move is made in the last case if the active loop is trivial.

- II. Re-route: We here want to change the  $O(N)$  contraction or line connectivity structure at  $u$ . We have to distinguish a few cases. In the cases not covered below no move is made.



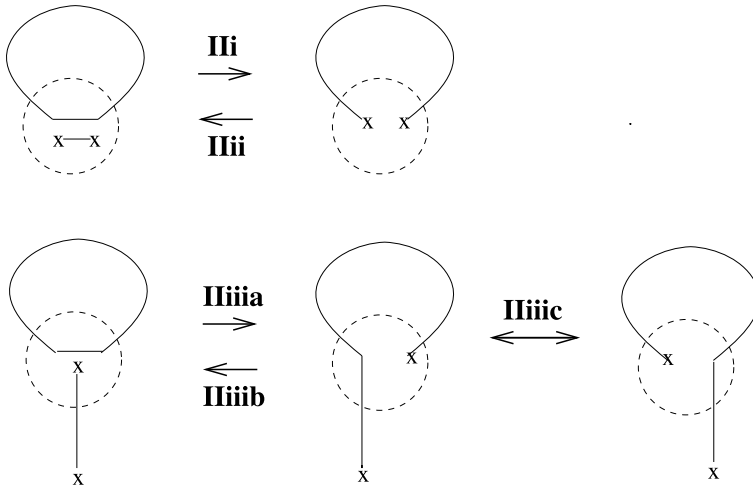


Fig. 2. Illustration for the re-routing moves. The dashed line encircles elements associated with one site. The  $x$  stand for the 1-vertices at  $u, v$  while a line both entering and leaving the dashed circle represents a 2-vertex. There could be more ‘spectator’ 2-vertices at the site which are not drawn for clarity.

- i. The active loop is trivial and  $d(u) > 2$ . In this case the we pick a 2-vertex at  $u$  and replace it by the two 1-vertices. The amplitude ratio is

$$q_{\text{rer}} = \frac{d[u] - 2}{N}. \tag{27}$$

Note that upon acceptance the active loop becomes non-trivial and the loop number  $|A|$  is reduced by one.

- ii. The active loop is not trivial but  $u = v$  holds. In this case we make the move inverse to i. Consequently the amplitude ratio is  $(q_{\text{rer}})^{-1}$ .
- iii. We have  $u \neq v$  and  $d(u) > 2$ . We pick with equal probability one of the lines connected to any of the 2-vertices at  $u$  and propose to redirect it to the 1-vertex. The line previously connected to the latter is rewired to the newly created ‘opening’ at the 2-vertex. For the amplitude ratio we need to distinguish further sub-cases. In Fig. 2 we give a hopefully helpful illustration of the various moves.
  - (a) The chosen 2-vertex belongs to a passive loop. The latter then gets inserted into the active loop,  $|A|$  is reduced by one, and the amplitude ratio is  $1/N$  in this case.
  - (b) The chosen 2-vertex belongs to the active loop, which self-intersects at  $u$ , and the chosen line leads towards the 1-vertex at  $v$ . In this case a new passive loop is detached and  $|A|$  goes up by one. The amplitude ratio is  $N$ .
  - (c) The chosen 2-vertex belongs to the active loop and the chosen line does not lead to the 1-vertex at  $v$ . In this case the active loop is just re-ordered and the amplitude ratio is one.

- III. Kick: Do nothing unless the active loop is trivial. If this is the case we pick a random site  $x$  and propose to move both  $u = v$  to  $x$ . The active loop remains trivial. The acceptance amplitude ratio is

$$q_{\text{kick}} = \frac{N + d[u] - 2}{N + d[x]}. \tag{28}$$

It should be easy to imagine now how the available information in the list  $\ell$  described before is useful during the update steps. For instance the active/passive flag helps to discriminate between the sub-cases of IIIii based on locally available information. It is also clear that precisely analogous steps can be defined around  $v$  instead of  $u$  chosen above. After some brief experiments we have arranged the updates in the following way

$$1 \text{ Iteration} := (I_u II_u I_v II_v III)^{N \times V/2}. \quad (29)$$

This was partly based on aesthetics and symmetry. For instance making only  $u$  steps or dropping III made little difference for our observables.<sup>7</sup> All Metropolis acceptance rates are well above 0.5 with the exception of the extensions step in I. The latter is close to  $(2D)^{-1}$ . For simulations with the modified action in Section 5 it will rise to 1 however.

The mathematical proof of ergodicity is the usual one: with a nonzero probability any configuration  $A$  can be transformed to the trivial empty one and then evolved to any other  $A'$ . It is also the empty lattice from which we start all simulations. Another observation is the following. A correct algorithm is also given with only the steps i and ii contained in II, thus re-routing only for  $u = v$ . We have indeed confirmed some correct results with such an update, but it is accompanied by severe critical slowing down. We shall see that this is completely eliminated by the additional steps.<sup>8</sup>

Observables are accumulated after each  $I_u$  and  $I_v$  step during the update. In most runs these contributions are stored separately for each iteration, and later an off-line autocorrelation analysis [14] is carried out for these time series. We then arrive at integrated autocorrelation times in units of iterations (29). During the mostly local steps needed to update the list  $\ell$  we sometimes have to trace a closed loop, for example to adjust the active/passive flag. Because of this it is not obvious at this point that the effort for one iteration scales strictly proportional to the lattice size  $V$ . We shall come back to this point in the next section.

#### 4. Numerical experiments with the standard action

We have first made series of runs for the loop model representing the standard lattice action discussed up to here. Most of these results can hence be directly compared to numbers in the literature. In Table 2 we have listed run parameters and the observed integrated autocorrelation times for a few observables. For the A-series the  $\beta$  values of [15] have been adopted together with lattice sizes to arrange for  $mL \approx 8$  to hold. According to [16] our massgap then differs from the infinite volume one only at the level of  $10^{-4}$  which will be below our errors. The weight  $\rho$  in (13) is chosen to roughly anticipate the decay of the two point function. The relative error of the true correlation (15) is then constant or even shrinking as we explore the exponential fall-off over a long range. We refer to the detailed discussion in [9] which applies here unaltered. In this paper we use the free massive lattice propagator to determine  $\rho$ ,

$$(-\Delta + \hat{M}^2)f(x) = \delta_{x,0} \Rightarrow \rho(x) = f(x)/f(0), \quad (30)$$

<sup>7</sup> If both is done,  $v$  does not move anymore. Observables where we average over translations still seemed to assume correct values.

<sup>8</sup> In the zoological interpretation as a worm algorithm [6] step I corresponds to the normal development of a worm. II deals with the asexual reproduction by detaching parts of its body (IIiib). Sadly, the  $O(N)$  worm sometimes also devours its offspring with probability  $1/N$  (IIiia).

Table 2

Run parameters and autocorrelation times. The statistics for each run consists of  $10^6$  iterations. For A, . . . , D the geometry is symmetric  $L_\mu \equiv L$ , while in E it is elongated in ‘time’,  $L_0 = 6L_1 \equiv 6L$ . The critical value  $\beta_c^{[17]} = 0.693002$  was taken from [17].

Run	$N$	$D$	$L$	$\beta$	$\hat{M}$	$\tau_{\text{int},K}$	$\tau_{\text{int},\chi}$	$\tau_{\text{int},m}$	$\tau_{\text{int}, \Delta }$	CPU
A <sub>1</sub>	3	2	56	1.4	$8L^{-1}$	1.84(3)	0.518(3)	0.678(6)	1.46(2)	1.50
A <sub>2</sub>	3	2	88	1.5	$8L^{-1}$	1.74(3)	0.515(3)	0.691(6)	1.39(2)	1.58
A <sub>3</sub>	3	2	152	1.6	$8L^{-1}$	1.72(3)	0.515(3)	0.698(6)	1.38(2)	1.75
A <sub>4</sub>	3	2	276	1.7	$8L^{-1}$	1.71(3)	0.514(3)	0.702(6)	1.37(2)	2.01
A <sub>5</sub>	3	2	518	1.8	$8L^{-1}$	1.65(3)	0.510(3)	0.689(6)	1.34(2)	2.56
B	8	2	128	5.2	$8L^{-1}$	1.94(3)	0.506(3)	0.571(4)	1.48(2)	2.51
C <sub>1</sub>	1	2	128	$\beta_c^{\text{ex}}$	$\rho \equiv 1$	2.42(6)	0.927(14)	–	2.41(6)	1.42
C <sub>2</sub>	1	2	256	$\beta_c^{\text{ex}}$	$\rho \equiv 1$	2.80(7)	1.005(16)	–	2.83(7)	1.49
D <sub>1</sub>	3	3	32	$\beta_c^{[17]}$	$\rho \equiv 1$	4.08(9)	0.818(8)	–	3.02(6)	1.50
D <sub>2</sub>	3	3	64	$\beta_c^{[17]}$	$\rho \equiv 1$	4.92(12)	0.910(10)	–	3.63(8)	1.83
E <sub>1</sub>	3	2	16	1.779	$2L^{-1}$	0.824(8)	0.536(4)	0.776(8)	0.72(1)	1.95
E <sub>2</sub>	3	2	32	1.779	$2L^{-1}$	0.900(10)	0.527(3)	0.842(9)	0.79(1)	2.21

Table 3

Values of some physical observables defined in the text. In the last column we cite references, where data consistent with the ones here can be found.

Run	$K$	$\chi$	$m^{-1}$	$\langle\langle  \Delta  \rangle\rangle_0 \times V^{-1}$	Ref.
A <sub>1</sub>	0.78701(8)	78.75(16)	6.876(5)	0.34590(4)	[15]
A <sub>2</sub>	0.90246(6)	175.38(41)	11.053(8)	0.34818(3)	[15]
A <sub>3</sub>	1.01715(4)	448.3(1.1)	19.030(13)	0.34604(2)	[15]
A <sub>4</sub>	1.12920(2)	1269.4(3.5)	34.530(25)	0.34244(1)	[15]
A <sub>5</sub>	1.23829(1)	3855(11)	64.872(66)	0.33927(1)	[15]
B	3.38678(6)	431.54(80)	18.096(9)	0.88431(3)	[18]
C <sub>1</sub>	0.31264(8)	$1.095(7)L^{7/4}$	–	0.13190(4)	[9]
C <sub>2</sub>	0.31217(5)	$1.104(8)L^{7/4}$	–	0.13216(3)	[9]
D <sub>1</sub>	0.23015(2)	$1.1055(19)L^2$	–	0.19294(1)	
D <sub>2</sub>	0.22910(1)	$1.0771(17)L^2$	–	0.193582(4)	
E <sub>1</sub>	1.2178(2)	242.1(1.4)	15.115(26)	0.33892(11)	[19]
E <sub>2</sub>	1.21662(9)	632.5(3.1)	25.115(37)	0.33867(5)	[19]

where  $\Delta$  is the standard nearest neighbor lattice Laplacian. Using the fast Fourier transform on one lattice direction after another, its construction costs negligible  $O[DL^D \ln D]$  operations. Thus the column for  $\hat{M}$  completely determines  $\rho(x)$ .

In Table 3 the corresponding mean values and errors are compiled. They refer to the mean bond occupation (19), the susceptibility (20), and the loop number appearing in (12). In addition we have recorded the two point function

$$G(t) = \langle\langle \rho(u-v)[\delta_{t,u_0-v_0} + \delta_{t,u_1-v_1}] \rangle\rangle. \quad (31)$$

In this formula, valid for the  $D = 2$  symmetric geometry, we sum over both directions and  $\delta$  is taken  $L$ -periodic. In addition we average over reflections. We have checked that these contributions are not completely, but largely statistically independent.

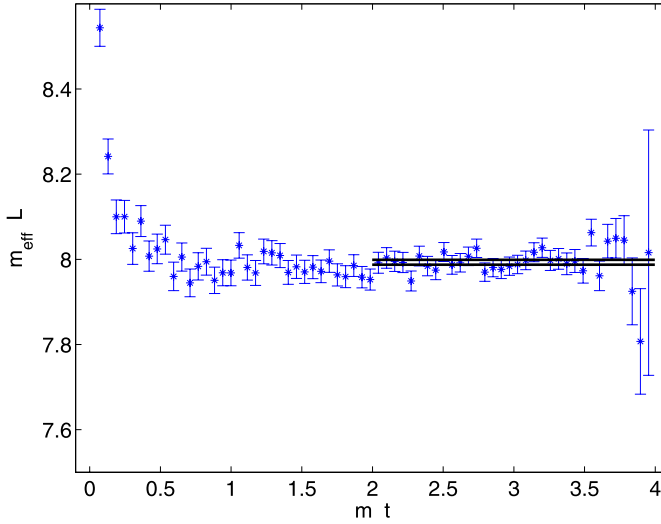


Fig. 3. Effective masses and fitted mass (band between the lines) from run A<sub>4</sub> ( $L = 276$ ). To avoid cluttering only every second  $m_{\text{eff}}$  is shown.

In Fig. 3 the errorbars show effective masses derived from the ratio of successive time-slice correlations by matching with  $\cosh(m_{\text{eff}}(t - L/2))$ . We see the expected long plateau and it seems completely safe from excited states errors to finally extract the mass from a fit, for which the horizontal line shows the range and the value in the form of an  $\pm 1\sigma$  error band. For the fit we have minimized over the shown range the function

$$X^2 = \sum_t \frac{[G(t) - c \cosh(m(t - L/2))]^2}{\delta G(t)^2} \tag{32}$$

with respect to  $c$  and  $m$ . More precisely, we first determine the error  $\delta G(t)$  by analyzing  $G(t)$ . As expected  $\delta G(t)/G(t)$  hardly grows with  $t$ . Then these errors are used to define via the minimization of (32)  $m$  as a function of the primary correlation data. An error for this derived observable is estimated as discussed in [14]. These are the values quoted for  $m$  in Table 3. Although the effective masses fluctuate around the plateau (see Fig. 3), the  $G(t)$  cannot be expected to be completely uncorrelated at neighboring  $t$  values. While (32) is the so-called uncorrelated  $X^2$  we actually see values between 0.1 and 0.4 per degree of freedom. This is not extremely small, we collect much more independent information than is customary in standard simulations. In fact the error of the fitted mass is between 2 (for A<sub>1</sub>) and 4 (for A<sub>5</sub>) times smaller than that of the effective mass at the beginning of the fit range alone. We have found that the mass values and their errors change only within their errors, if we replace the weight  $\delta G^{-2}$  in (32) by one flat in  $t$ . Plots similar to Fig. 3 arise for all lattices where a mass is quoted. The data in [15] allow to roughly estimate which statistics was invested for the errors quoted in units of steps per spin. We conclude that for the estimation of the mass gap, the present method is quite competitive with the reflection cluster algorithm [4] with improved estimator [15]. This is not quite so for  $\chi$ , which could possibly profit from a different choice of  $\rho$ .

In the series C we investigate the exactly solved two dimensional Ising model by simply setting  $N = 1$  in our loop code. The efficiency is in fact quite similar to the simulations in [9] although the sampling of the contraction structures in (13) is an in principle unnecessary com-

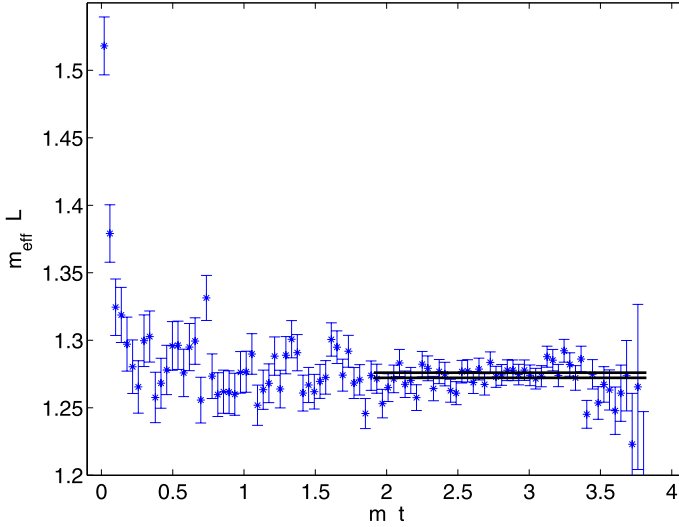


Fig. 4. Similar to Fig. 3, but for simulation  $E_2$  ( $L_0 = 192$ ,  $L_1 = 32$ ).

plication as  $N^{|A|}$  equals unity in this case, see Appendix A for further remarks. In the series D we take the O(3) model to three dimensions and simulate at the critical point  $\beta = 0.693002$  determined in [17]. Beside the two runs quoted we have also reproduced data from [20]. The C and D cases demonstrate the very mild critical slowing down of our simulations at criticality where  $L$  is the only scale.

With E we turn to studies of the renormalized coupling

$$\bar{g}^2 = m(L)L \quad (N = 3) \quad (33)$$

that has been introduced in [1]. Here  $m(L)$  is the mass gap of the transfer matrix of spatial size  $L$ . In [1] it was argued that at least in the perturbative regime free boundary conditions in the time direction help to isolate the first excited state from the rest of the spectrum. The loop model could easily be modified to these boundary conditions. We here prefer however to make the time direction long ( $L_0 = 6L$ ) to achieve the isolation. This is facilitated again by our small errors at large separation. An advantage of this approach is that exact translation invariance is kept for both directions. In Fig. 4, analogous to 3, we demonstrate how the gap is extracted also in this case. Here we took  $\hat{M} > m$  and correspondingly ‘oversample’ [9] large distances with errors shrinking with growing  $t$  (except very close to  $L_0/2$ ). Recently in [21] and [19] a thorough study of cutoff effects in the step scaling function for (33) was made. In this context very accurate data were produced including our lattices  $E_1, E_2$  where we obtain  $\bar{g}^2 = 1.0586(18)$  and  $\bar{g}^2 = 1.2741(19)$ . In this case a special estimator [22] is available in the spin formulation such that our accuracy achieved here cannot really compete with [19], but the more accurate values are consistent with ours.

We now make some general observations on the loop configurations observed in our runs.

An exceedingly encouraging observation on our compiled autocorrelation times is, that in units of iterations there seems to be almost no critical slowing down for any of the series and quantities studied here. The typical bond occupations  $K$  resemble  $E$ , see (19), and are functions of  $\beta$  with only a weak dependence on  $L_\mu$ . They are larger in lower dimension. The number of

loops  $|A|$  is strictly proportional to  $V$  and also similar to  $E$ . Both quantities grow with  $N$  for similar correlation lengths as one would expect.

We finally return to the question of the computational complexity of one iteration. Here the last column ‘CPU’ in Table 2 is of interest. It gives the execution time in  $\mu$  sec of one micro step, i.e. the time for one iteration divided by  $NV$ . This is of course a highly non-universal implementation and processor dependent quantity of not much interest. It is quoted however, because its relative change between the runs may be of some more interest. A constant value for CPU would suggest a scaling behavior like for sweeps of local algorithms. The additional growth that we see within the simulation series represents a small effective slowing down in CPU time units. In the A series we really take a scaling limit. From  $A_1$  to  $A_5$  the correlation length changes by a factor 9.4. The extra CPU time factor is 1.7. The reason for this extra growth indeed comes from the ‘looping’ steps as discussed at the end of the last section. For a discussion of the true asymptotic dynamical behavior, where this component will probably eventually dominate, one could investigate the distribution and scaling behavior of the perimeters of the loops in analogy to percolation cluster sizes. We however do not try to determine dynamical exponents. We just conclude that the new type of simulations is efficient enough to generate all data cited here in a few hundred hours on a PC with a code that still allows for ample speedup. It is not clear at the moment if a modified list parameterization and/or algorithm could avoid this more than linear with the lattice volume growth of the CPU time per iteration. Note that we have been discussing the continuum limit throughout. For the thermodynamic limit ( $V \rightarrow \infty$  at fixed  $\beta$ ) strict linearity is expected for the massive theory.

We close by a few remarks about our specific implementation that is reflected in the quantity CPU. Our code is written in and running under `matlab`. Only the random numbers are imported from the C-code [23] and we use luxury level two throughout. We used up-to-date (2008) PCs with four cores that we employ for trivial parallelization thus speeding up the time following from Table 2 by a factor four. We hence always have four replica which allow for another reassuring consistency check on the error determination by always monitoring the  $Q$ -values [14]. It would be clearly possible to speed up our runs by a large factor by writing a dedicated C-code. In particular the data type ‘pointer’ seems ideal for the handling of loops by lists. Like for cluster simulations, the present algorithm presumably does not lend itself very naturally to a non-trivial parallelization.

## 5. Simplified actions

For the  $O(N)$  model we have succeeded to simulate the untruncated strong coupling expansion for the standard nearest neighbor lattice action. This could be achieved because the weight needed to integrate out the spins (3) is relatively simple in this case. We anticipate that in other models that we shall want to treat similarly this may be more involved. It would be easier to handle the graphs and to tabulate the required weights if we could limit the overlapping of loops. For the  $O(N)$  model this would amount to constraining the sum in (5) and in the formulae following from it by

$$k(l) = 0, 1, 2, \dots, k_{\max}. \quad (34)$$

In the simulations reported above the single link occupations  $k(l)$  exhibit a Poisson type distribution. Hence, for the mean values given, they never get much beyond about 10 and a  $k_{\max}$  of this size would have very little effect. From here on we shall however investigate the most radical

possibility by setting  $k_{\max} = 1$ . Then we effectively replace (1) by

$$\tilde{Z}(u, v) = \int \left[ \prod_z d\mu(s(z)) \right] s(u) \cdot s(v) \prod_{l=(xy)} [1 + \tilde{\beta}s(x) \cdot s(y)] \tag{35}$$

and use a tilde for quantities which refer to this action. It is clearly still ultralocal and, if such a system becomes critical at all, we would expect to be in the same universality class as before. The Boltzmann factor is strictly positive for  $|\tilde{\beta}| < 1$  only. In the Ising model at  $N = 1$  the truncation  $k_{\max} = 1$  is related to expanding in  $\tilde{\beta} = \tanh \beta$  instead of  $\beta$ . Then, with this identification, we compute exactly the same correlations on every finite lattice.

A weight like (35) is actually not new in the literature. In [24] this action was put on a honeycomb lattice in two dimensions. Since only three links meet at a site there, the strong coupling graphs simplify as they cannot overlap or intersect, similarly to the Majorana fermions in [10]. In this way relations with certain discrete models can be derived. This is elaborated in [25] where critical indices are derived for  $-2 \leq N \leq 2$ . In both publications it is conjectured that, although unusual, the Boltzmann weight in (35) should lead to the  $O(N)$  universality class. We here check this for the  $O(3)$  model in  $D = 2$  (on our usual square lattice) by computing the step scaling function (SSF) of [1].

It involves pairs of lattices

$$\Sigma(2, u, L^{-1}) = m(2L)2L \Big|_{m(L)L=u} \tag{36}$$

where the side condition determines the value  $\beta$  (or  $\tilde{\beta}$ ) to be used on both lattices. For each  $u$  the SSF is expected to have a universal continuum limit

$$\sigma(2, u) \equiv \Sigma(2, u, 0) = \lim_{L \rightarrow \infty} \Sigma(2, u, L^{-1}) \tag{37}$$

where  $\sigma$  is equivalent to the Callan Symanzik beta function for the renormalization scheme defined by the coupling (33). It is quite amazing that by Bethe Ansatz techniques the continuum SSF  $\sigma$  could be computed exactly [26]. For our universality check we pick the particularly popular point [1,19]

$$\bar{u}_0 = 1.0595, \quad \sigma(2, \bar{u}_0) = 1.261210. \tag{38}$$

The exact result has been confirmed with extreme numerical precision in [19].

A few short experiments immediately showed that  $\tilde{\beta} > 1$  is required to achieve any sizable correlation length in lattice units. Then the weight in (35) oscillates and presumably has a severe ‘sign problem’. The loop partition function  $\tilde{Z}$  which is just as (11) but omitting terms with any  $\tilde{k}(l) > 1$  continues to be a sum of positive terms, of course. It is also plausible that loops in  $\Lambda$  grow with rising  $\tilde{\beta}$  and thus encode correlations of growing range. The counterpart of (19) now reads

$$\tilde{K} = \frac{1}{N_l} \sum_l \langle \tilde{k}(l) \rangle_0 = \frac{1}{N_l} \sum_{l=(xy)} \left\langle \frac{\tilde{\beta}s(x) \cdot s(y)}{1 + \tilde{\beta}s(x) \cdot s(y)} \right\rangle. \tag{39}$$

In the scaling region we shall find mean bond occupations not far from 1/2. Due to the non-positive weight it is however not possible to draw any immediate conclusions on the nature of ‘typical’ field configurations in the spin representation. It also seems hard to imagine to set up a bare perturbative expansion on the lattice with this action. This is perhaps somewhat reminiscent of the constraint model in [27] where the Boltzmann factor acts ferromagnetically only in the

Table 4

Lattice data with  $k_{\max}=1$  for the O(3) model in  $D = 2$  with  $L_0 = 6L_1 \equiv 6L$ . Each line represents  $3 \times 10^6$  iterations.

$L$	$\tilde{\beta}$	$\tilde{K}$	$\langle  \tilde{A}  \rangle_0 \times V^{-1}$	$\tilde{g}^2$	$\tilde{\beta}(\tilde{u}_0)$	CPU
6	4.4400	0.41727(6)	0.09134(3)	1.0580(6)	4.4263(58)	2.03
8	4.8661	0.44018(4)	0.08406(3)	1.0586(6)	4.8565(67)	2.07
12	5.6803	0.47652(3)	0.08022(2)	1.0592(6)	5.6770(85)	2.18
16	6.4511	0.50556(2)	0.07949(2)	1.0625(7)	6.4949(99)	2.23
24	7.9210	0.55362(2)	0.07978(1)	1.0566(7)	7.873(12)	2.37
50	10.7408	0.63815(1)	0.08093(1)	1.0585(9)	10.722(16)	3.07

Table 5

The doubled lattices of Table 4,  $10^6$  iterations each.

$L$	$\tilde{\beta}$	$\tilde{K}$	$\langle  \tilde{A}  \rangle_0 \times V^{-1}$	$\tilde{g}^2$	$\Sigma(2, \tilde{u}_0, 1/L)$	CPU
12	4.4294	0.41595(5)	0.07764(3)	1.1784(11)	1.1788(13)	2.05
16	4.8661	0.43977(4)	0.07723(3)	1.1892(11)	1.1903(13)	2.14
24	5.6765	0.47622(2)	0.07766(2)	1.2124(11)	1.2123(14)	2.24
32	6.4899	0.50682(2)	0.07844(2)	1.2269(12)	1.2265(14)	2.36
48	7.8716	0.55202(1)	0.07943(1)	1.2432(13)	1.2431(15)	2.61
100	10.7408	0.63813(1)	0.08091(1)	1.2578(15)	1.2591(18)	3.58

form of a step function on the angle between neighboring spins. If features of the long range physics are nevertheless described by renormalized perturbation theory, this must be viewed more like an effective field theory matched to these lattice models.

We now come to our concrete data taken allowing  $k(l) = 0, 1$  only. For the SSF we have to first determine the values  $\tilde{\beta}$  that yield  $\tilde{g}^2 = \tilde{u}_0$  on a series of lattices. Such results are listed in Table 4. We have measured the derivative  $\partial\tilde{g}^2/\partial\tilde{\beta}$  and used it to solve the problem of tuning  $\tilde{\beta}$  (6th column). Our simulations are so close to the target that further terms in a Taylor expansion and the errors of the measured derivative play no rôle. We note that  $\tilde{\beta}$  gets rather large and that there are about four times fewer loops than in  $E_{1,2}$  before. The effective mass plots were again inspected. They all look qualitatively indistinguishable from Fig. 4. Again  $\hat{M} = 2/L$  determined  $\rho(u - v)$  for us.

In Table 5 we list the corresponding doubled lattices required for the SSF. We notice that  $\tilde{\beta}$  differs slightly from the values in column 6 of Table 4. This has technical reasons and this tiny shift is again taken into account in  $\Sigma$  by using  $\partial\tilde{g}^2/\partial\tilde{\beta}$ . The error quoted for  $\Sigma(2, \tilde{u}_0, 1/L)$  combines the statistical errors of both the small and the doubled lattice.

In Fig. 5 we plot our SSF data. The left panel shows  $\Sigma$  versus  $L^{-2}$  with the star at zero giving the exact continuum limit [26]. It is very obvious that the data deriving from the action in (35) ‘know’ about the universal value. In [19] a detailed investigation on the Symanzik effective field theory for the lattice artifacts in the two dimensional O(N) models was carried out. The result is that the leading term for O(3) is expected to be of the form  $\ln^3 L/L^2$  with subleading contributions having smaller powers of the logarithm. This has motivated us to plot  $(\Sigma - \sigma)L^2/\ln^3 L$  versus  $\ln^{-1} L$ . The two lines are quadratic polynomials in  $\ln^{-1} L$  representing fits with acceptable  $\chi^2$  values. The dashed line differs from the solid one by including/omitting the coarsest lattice pair. We see how plotting matters: what is a short extrapolation in the left plot is an uncomfortably long one in the right panel. But the artifacts for our action are clearly compatible with the theoretical form. In addition it is reassuring to note that any non-absurd extrapolation in



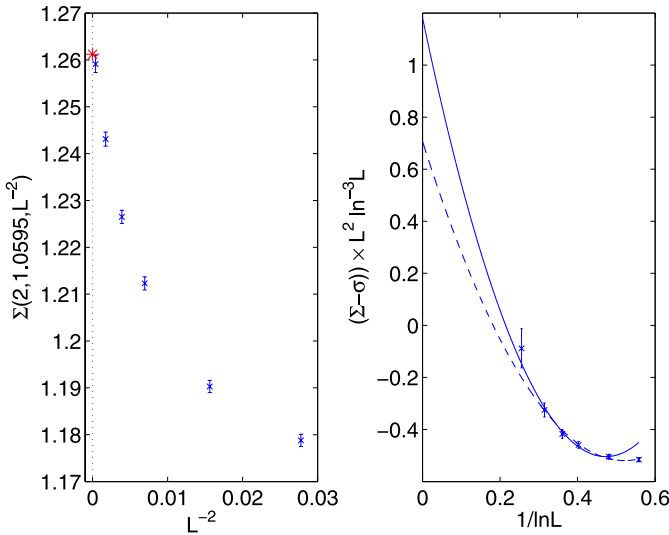


Fig. 5. Data for the step scaling function with the  $k_{\max} = 1$  action. The star in the left plot is the known exact answer. The right plot is relevant for the theory of scaling violations à la Symanzik in [19].

the left plot would not miss the continuum value by much. Taking just the finest lattice would be low by less than 2 permille, comparable to our statistical error.

## 6. Conclusions and outlook

We have successfully extended the method of simulating strong coupling graphs instead of fields to the  $O(N)$  models. They are in this way first reformulated as a loop model which is then simulated. The resulting setup of reformulation plus algorithm is, at least for the mass gap as an observable, similarly efficient as the reflection cluster method. A variant of the lattice Boltzmann factor, suggested by simplifying the loop ensemble, was simulated and demonstrated to yield the same continuum step scaling function for a particular value of the coupling. Hence universality is confirmed here in an interesting case. A direct simulation as a spin model would presumably be difficult due to sign oscillations of the Boltzmann weight.

The main goal of this work was not primarily to have another simulation method for the  $O(N)$  models. The main motivation was that the further extension of this technique is possible in a more systematic way than for the cluster method. After all, many systems possess a strong coupling expansion. The  $O(N)$  model is simply a very well studied case which has taught us important lessons about the general approach. As a byproduct one could now however study the  $O(N)$  models for non-integer  $N$  and perhaps one could also consider taking the  $N \rightarrow \infty$  limit (at fixed  $\beta/N$ ) of the algorithm similarly to the time continuum limit in [28]. Also, as already indicated above, the study of the individual loop distribution in the spirit of percolation theory could be of some interest.

A modest next step in the main line of the project will be to consider  $CP(N - 1)$  spin models, for which no efficient cluster algorithm exists, at least for the classical models (see however [29]). A more long distance goal remains the simulation of lattice gauge theory as an equivalent surface model.

### Acknowledgements

I would like to thank Martin Hasenbusch, Erhard Seiler, Rainer Sommer and Peter Weisz for discussions and help with the literature as well as Burkhard Bunk for advice with the computers. Financial support of the DFG via SFB transregio 9 is acknowledged.

### Appendix A. The Ising limit $N = 1$

For  $N = 1$  the  $O(N)$  system becomes the Ising model. In this case the function (3) is  $G_1(j) = \cosh(j)$  and hence

$$c(n; 1) = \frac{1}{(2n)!} \tag{40}$$

such that

$$\prod_z c[d(z)/2; 1] = \frac{1}{\mathcal{M}_0} \tag{41}$$

may be used in (12). With no more dependence on  $|A|$

$$\mathcal{Z} = \sum_{\Lambda \in \mathcal{L}_2} \rho^{-1}(u - v) \frac{\mathcal{M}[u, v; k]}{\mathcal{M}_0[u, v; k]} \left[ \prod_l \frac{\beta^{k(l)}}{k(l)!} \right] \tag{42}$$

may be rewritten as a sum over  $u, v, k$

$$\mathcal{Z} = \sum_{u, v, k} \rho^{-1}(u - v) \left[ \prod_l \frac{\beta^{k(l)}}{k(l)!} \right] \prod_x \delta_{d(x), \text{even}} \tag{43}$$

which is the expected  $\beta$  expansion for the Ising model. Note that  $u, v$  enter via the relation (7). While the form (11) contains the sum over different contractions it is also correct with  $N = 1$ . All contractions are equally likely in this case, the sum over them factorizes off.

It is interesting to interpret our general update from the point of view of the ensemble (43). To obtain the effective transition probability from step I we average over possible contractions at  $u$  and sum over the resulting ones at  $\tilde{u}$ . This leads (for  $\rho \equiv 1$ ) to the following update sequence

- With probability  $1 - 1/(2D + 1)$ :
  - Pick a link  $l = \langle u\tilde{u} \rangle$  around  $u$  in one of the  $2D$  directions with equal probability.
  - Move  $u \rightarrow \tilde{u}$  [and  $k(l) \rightarrow k(l) + 1$ ] with probability  $\min[1, \beta/(d(\tilde{u}) + 1)]$ .
- With probability  $1/(2D + 1)$ :
  - Pick a link  $l = \langle u\tilde{u} \rangle$  around  $u$  in one of the  $2D$  directions with probability  $k(l)/(d(u) - 1)$ . These probabilities add up to unity for the  $2D$  link directions if  $u \neq v$  holds. For  $u = v$  there is a probability  $1/(d(u) - 1)$  that no direction is picked. In this case no move is made.
  - Otherwise move  $u \rightarrow \tilde{u}$  [and  $k(l) \rightarrow k(l) - 1$ ] with probability  $\min[1, (d(u) - 1)/\beta]$ .

The ratio in the third sub-item is the fraction of all possible pairings that connects  $u$  to a link in the given direction. It is not hard to see that these implied transitions for  $u, v, k$  obey detailed balance with respect to (43).

## References

- [1] M. Lüscher, P. Weisz, U. Wolff, A numerical method to compute the running coupling in asymptotically free theories, Nucl. Phys. B 359 (1991) 221.
- [2] M. Lüscher, R. Narayanan, P. Weisz, U. Wolff, The Schrödinger functional: A renormalizable probe for non-Abelian gauge theories, Nucl. Phys. B 384 (1992) 168.
- [3] R.H. Swendsen, J.-S. Wang, Nonuniversal critical dynamics in Monte Carlo simulations, Phys. Rev. Lett. 58 (1987) 86.
- [4] U. Wolff, Collective Monte Carlo updating for spin systems, Phys. Rev. Lett. 62 (1989) 361.
- [5] S. Caracciolo, R.G. Edwards, A. Pelissetto, A.D. Sokal, Wolff type embedding algorithms for general nonlinear sigma models, Nucl. Phys. B 403 (1993) 475.
- [6] N. Prokof'ev, B. Svistunov, Worm algorithms for classical statistical models, Phys. Rev. Lett. 87 (2001) 160601.
- [7] M. Lüscher, Trivializing maps, the Wilson flow and the HMC algorithm, arXiv:0907.5491 [hep-lat].
- [8] H.A. Kramers, G.H. Wannier, Statistics of the two-dimensional ferromagnet. Part I, Phys. Rev. 60 (1941) 252.
- [9] U. Wolff, Simulating the all-order strong coupling expansion I: Ising model demo, Nucl. Phys. B 810 (2009) 491.
- [10] U. Wolff, Simulating the all-order hopping expansion II: Wilson fermions, Nucl. Phys. B 814 (2009) 549.
- [11] O. Bär, W. Rath, U. Wolff, Anomalous discrete chiral symmetry in the Gross–Neveu model and loop gas simulations, Nucl. Phys. B 822 (2009) 408.
- [12] U. Wolff, Precision check on triviality of  $\phi^4$  theory by a new simulation method, Phys. Rev. D 79 (2009) 105002.
- [13] C. Itzykson, J.M. Drouffe, Statistical Field Theory, vol. 2, Cambridge University Press, 1989.
- [14] U. Wolff, Monte Carlo errors with less errors, Comput. Phys. Commun. 156 (2004) 143.
- [15] U. Wolff, Asymptotic freedom and mass generation in the O(3) nonlinear sigma model, Nucl. Phys. B 334 (1990) 581.
- [16] M. Lüscher, On a relation between finite size effects and elastic scattering processes, Lecture given at Cargese Summer Inst., Cargese, France, 1 September 1983.
- [17] Y. Deng, H.W.J. Blöte, M.P. Nightingale, Surface and bulk transitions in three-dimensional O( $n$ ) models, Phys. Rev. E 72 (1) (2005) 016128.
- [18] U. Wolff, Asymptotic scaling in 2-D O( $n$ ) nonlinear sigma models, Phys. Lett. B 248 (1990) 335.
- [19] J. Balog, F. Niedermayer, P. Weisz, The puzzle of apparent linear lattice artifacts in the 2d non-linear sigma-model and Symanzik's solution, arXiv:0905.1730 [hep-lat], Nucl. Phys. B, in press.
- [20] C. Holm, W. Janke, Critical exponents of the classical three-dimensional Heisenberg model: A single-cluster Monte Carlo study, Phys. Rev. B 48 (1993) 936.
- [21] J. Balog, F. Niedermayer, P. Weisz, Logarithmic corrections to O( $a^2$ ) lattice artifacts, Phys. Lett. B 676 (2009) 188.
- [22] M. Hasenbusch, An improved estimator for the correlation function of 2-D nonlinear sigma models, Nucl. Phys. B (Proc. Suppl.) 42 (1995) 764.
- [23] M. Lüscher, <http://luscher.web.cern.ch/luscher/ranlux>.
- [24] E. Domany, D. Mukamel, B. Nienhuis, A. Schwimmer, Duality relations and equivalences for models with O( $N$ ) and cubic symmetry, Nucl. Phys. B 190 (1981) 279.
- [25] B. Nienhuis, Exact critical point and critical exponents of O( $n$ ) models in two-dimensions, Phys. Rev. Lett. 49 (1982) 1062.
- [26] J. Balog, A. Hegedus, TBA equations for excited states in the O(3) and O(4) nonlinear sigma-model, J. Phys. A 37 (2004) 1881.
- [27] M. Hasenbusch, O( $N$ ) and  $\text{RP}^{N-1}$  models in two-dimensions, Phys. Rev. D 53 (1996) 3445.
- [28] B.B. Beard, U.J. Wiese, Simulations of discrete quantum systems in continuous Euclidean time, Phys. Rev. Lett. 77 (1996) 5130.
- [29] B.B. Beard, M. Pepe, S. Riederer, U.J. Wiese, Efficient cluster algorithm for CP( $N - 1$ ) models, Comput. Phys. Commun. 175 (2006) 629.